EUROPEAN ORGANIZATION FOR NUCLEAR RESEARCH
European Laboratory for Particle Physics

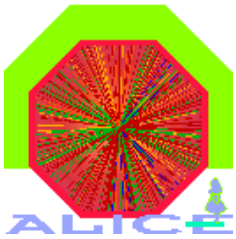

Internal Note/
ALICE reference number
ALICE-INT-2005-016 version 1.0
Institute reference number
[-]
Date of last change
2005-07-01

Bayesian approach for the identification of particles detected with PHOS

Authors:

G.Conesa[1], H.Delagrange[2], J.Diaz[1], Y.Karlov[3], Y.Schutz[2,4]

[1]IFIC (Centro Mixto Universidad de Valencia-CSIC), Valencia, Spain
[2]SUBATECH, UMR6457 (Ecole des Mines-IN2P3/CNRS-Université de Nantes), BP20722, 44307 Nantes CEDEX 3, France
[3]Institute for High Energy Physics, Protvino, Russia
[4]CERN, Geneva, Switzerland

Abstract:

The ALICE experiment at LHC will detect and identify photons, electrons and light neutral-mesons with the PHOS detector. We present a particle identification method, based on the Bayes theory of probabilities, enabling to complement within the PHOS acceptance the ALICE global particle identification.

Bayesian approach for the identification of particles detected with PHOS

1st July 2005

G. Conesa[1], H. Delagrange[2], J. Díaz[1], Y. Kharlov[3], Y. Schutz[2,4]

Abstract

The ALICE experiment at LHC will detect and identify photons, electrons and light neutral-mesons with the PHOS detector. We present a particle identification method, based on the Bayes theory of probabilities, enabling to complement within the PHOS acceptance the ALICE global particle identification.

Contents

[1]IFIC (Centro Mixto Universidad de Valencia-CSIC), Valencia, Spain

[2]SUBATECH, UMR6457 (Ecole des Mines-IN2P3/CNRS-Université de Nantes), BP20722, 44307 Nantes CEDEX 3, France

[3]Institute for High Energy Physics, Protvino, Russia

[4]CERN, Genève, Switzerland

Introduction

The high energy resolution spectrometer PHOS (PHOton Spectrometer) has been designed to provide excellent particle identification (PID) for photons, electrons and neutral mesons in a wide energy domain, ranging from several hundreds of MeV to above hundred GeV. PHOS (for detail, see [1–7]) consists of a calorimeter (EMC) and a charged particle veto detector, CPV.

PID methods with PHOS have already been presented previously [3, 4, 7, 8]. They are based on methods deriving the PID by combining all relevant information delivered by the detectors and provide, on a statistical basis, PID classes defined according to the value of the photon identification efficiency and the fraction of wrongly identified particles. With the new method, based on the Bayes theory of probabilities and discussed in the present note, PID weights are assigned, on an event-by-event basis, to every reconstructed particle. Combining these weights with similar PID weights derived from the ALICE central tracking system provides a global PID of all particles, both charged and neutral, emitted within the PHOS acceptance.

1 Bayesian method applied to PHOS data

The PID of particles detected with PHOS relies on three independent identification parameters derived from the data collected by the detectors:

1. the time-of-flight (tof),
2. the distance between the CPV and the calorimeter (d_{CE}),
3. and the lateral dispersion of the shower which develops in the calorimeter (dis).

In the Bayesian method, discussed here, PID weights are assigned to each reconstructed particle. The weights represent the probability that the detected particle is of a given type, among photon γ, electron $e^{\pm}$, charged hadron $h^{\pm}$, neutral hadron h^0 and high-p_T π^0. The weights are calculated according the following steps:

- First, charged ($\pi^{\pm}$, $k^{\pm}$, $\bar{p}$ and p) and neutral (K^0_L, $\bar{n}$ and n) hadrons are generated with realistic exponential energy distribution and tracked through the ALICE detection systems using the ALICE simulation tools, AliRoot [9]. Since, at variance with the previously listed hadrons, photons and high-p_T π^0(generating a single

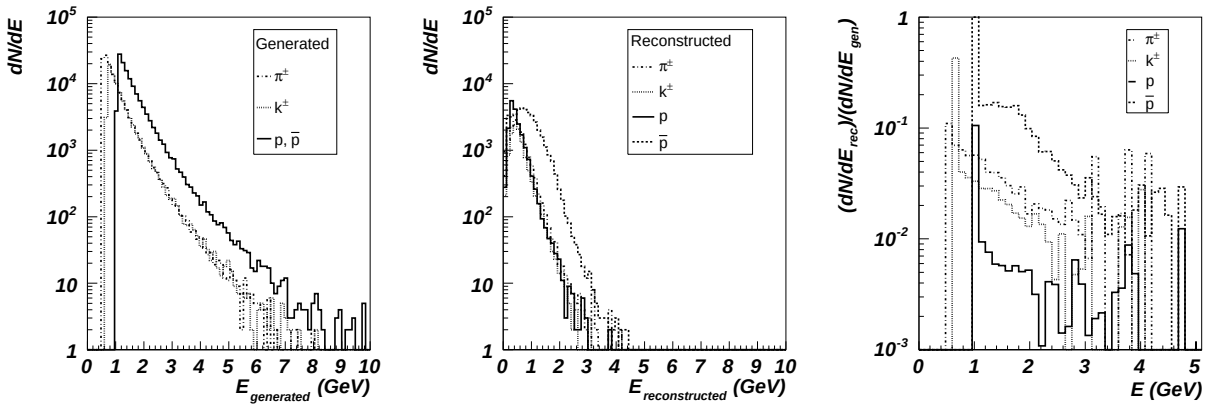

Figure 1: Generated (left) and reconstructed (middle) energy distribution in PHOS for charged hadrons. Right: ratio of the reconstructed to the generated energy distributions. Results for neutral hadrons are similar.

electromagnetic cluster in PHOS) always develop an electromagnetic shower in the calorimeter, they can be generated with an uniform energy distribution. The reconstructed particle spectra (Fig. 1) constitute the particle response function of the detector and are used as input of the next step.

- The density distribution, $P(\text{parameter}\,|\,\text{particle type})$, of the probability to identify a given particle type is calculated for each particle in the above list and for each one of the three identification parameters, *tof*, d_{CE} and *dis* (see Sec. 2). Either Landau[5] or Gaussian,

$$G(x) = c \cdot e^{-\frac{1}{2}\left(\frac{x-\mu}{\sigma}\right)^2}, \tag{1}$$

distributions are used to parameterize these distributions. Combining the probability obtained for each identification parameter, the final weights are calculated (see Sec. 3) giving the probabilities for a reconstructed particle to be of the types listed above.

- Finally, the method is tested by applying the algorithm to particles in HIJING [11] events and in events with a single photon, electron or high-energy π^0 merged in a HIJING event simulating a realistic heavy-ion collision environment (see Sec. 4).

[5]Landau distribution is defined by Root (Ref. [10]) as $L(x) = c \cdot f(\mu, \sigma, x)$, where μ is the most probable value of the distribution, σ is related to the width of the distribution and c is a constant parameter.

Particle	Function	c	μ (ns)	σ (ns)
γ, $e^{\pm}$	Gaussian	$7.83 \cdot 10^8$	1.55	$5.09 \cdot 10^{-2}$
$\pi^{\pm}$	Gaussian	$6.73 \cdot 10^8$	1.58	$5.87 \cdot 10^{-2}$
kaon	Gaussian	$3.93 \cdot 10^8$	1.64	$6.07 \cdot 10^{-2}$
kaon	Landau	$2.00 \cdot 10^9$	1.68	$4.10 \cdot 10^{-2}$
nucleon	Gaussian	$2.02 \cdot 10^8$	1.73	$9.52 \cdot 10^{-2}$
nucleon	Landau	$1.10 \cdot 10^9$	1.74	$1.00 \cdot 10^{-1}$

Table 1: Parameters obtained after fitting the time-of-flight probability density distributions for different particle species. Kaons and nucleons were fitted by a Gaussian distribution from the right of the distribution to its maximum and by a Landau distribution from their maximum to the left. The distributions are integrated from 0 to 2 GeV reconstructed energy.

2 Probability density distributions

2.1 Time of flight

Massive hadrons can be identified and discriminated from electrons and photons by measuring their time-of-flight (tof) from the collision vertex to PHOS. The measurement is discriminating up to transverse momenta of about 2 GeV. For larger values, all particles flight with almost the speed of light and cannot be discriminated anymore. Therefore, the tof parameter will be considered for PID only for particles with a reconstructed energy smaller than 2 GeV. However, the tof discriminating power will be limited by hadrons with transverse momenta larger than 2 GeV showering in the calorimeter and depositing only a fraction of their energy.

The tof probability density distributions, $P(tof \mid i)$, (Fig. 2) are calculated as the tof distribution for the particle of type i (as listed in the previous section), and for all reconstructed energy up to 2 GeV. The distributions are normalized to the total number of reconstructed events. The distributions are then parameterized (Tab. 1) with either a Gaussian or a Gaussian plus a Landau distribution (in the case of kaons and nucleons).

2.2 CPV-EMC distance

Electrons can be distinguished from other charged particles by measuring the distance between the impact of the particle in CPV and the impact in EMC. The probability density distributions (Fig. 3) , $P(d_{CE} \mid i)$, are calculated for the d_{CE} components projected to the PHOS surface, parallel to the beam axis (z) and perpendicular to the beam axis (x)[6] distance and for electrons, pions, kaons and anti-protons reconstructed with different energy values. For low reconstructed energies and for a given value of the energy, the measured x-component of the distance, d_{CE}^x, is larger for electrons than for hadrons. This is due to the fact that the electron energy is well measured with PHOS, whereas for hadrons

[6] Charged particles are bent in the direction of the x-axis.

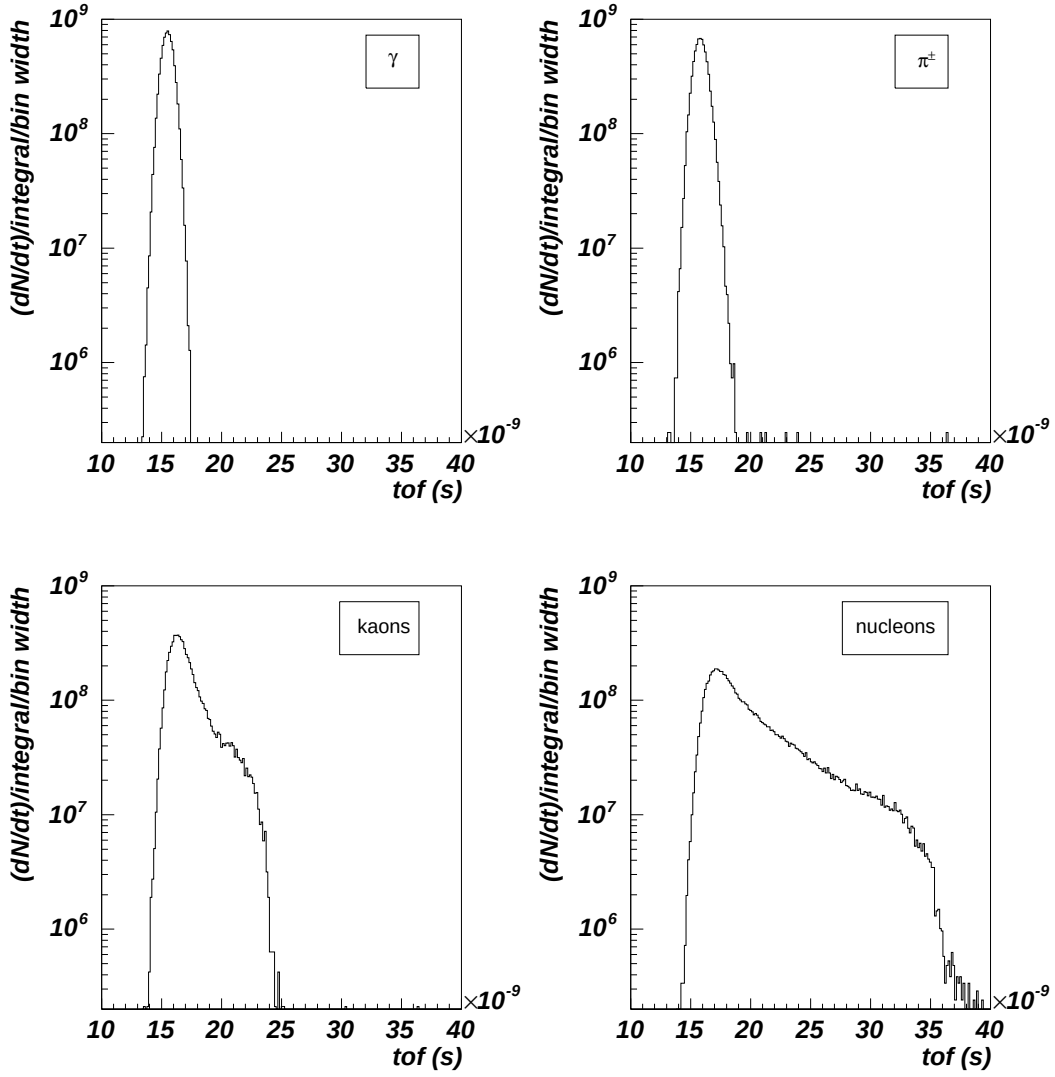

Figure 2: Time-of-flight probability density distributions for different particle species, photons (upper-left), charged pions (upper-right), kaons (lower-left) and nucleons (lower-right), integrated from 0 to 2 GeV reconstructed energy.

	p_0	p_1	p_2
	electrons	x-axis	
c_x	$-1.6 \cdot 10^{-2}$	0.77	-0.15
μ_x	0.35	0.25	4.12
σ_x	0.30	0.11	0.16
	electrons	z-axis	
c_z	0.49	0.53	$-9.8 \cdot 10^{-2}$
μ_z	$2.8 \cdot 10^{-2}$	$5.0 \cdot 10^{-2}$	$-8.2 \cdot 10^{-2}$
σ_z	0.25	$-1.7 \cdot 10^{-2}$	0.17
	$h^{\pm}$	x-axis	
c_x	0.14	$-3.0 \cdot 10^{-2}$	0
μ_x	1.4	$-9.3 \cdot 10^{-2}$	1.4
σ_x	5.7	0.27	-1.8
	$h^{\pm}$	z-axis	
c_z	0.46	-0.65	0.52
μ_z	$1.1 \cdot 10^{-2}$	0	0
σ_z	0.60	$-8.2 \cdot 10^{-2}$	0.45

Table 2: Parameters of the energy dependence of the probability density distributions calculated for charged hadrons and electrons and for the x- and z-component of the distance between the impact on CPV and on EMC.

only a fraction of the energy is measured, so that a low reconstructed energy originates from more energetic hadrons whose track has a small curvature. In addition, the measured fluctuation of the z-component, d_{CE}^z, distributions is smaller for electrons than for charged hadrons because hadronic showers cannot be as well localized as electromagnetic showers in PHOS.

The distributions are parameterized with Gaussian distributions. The variation of the Gaussian parameters with the reconstructed energy (Fig. 4) is described by a second-order polynomial of $1/E$, $p_0+p_1/E^2+p_2/E$, for the μ and σ parameters and by a parabola for the constant parameter. The parameters of the polynomial and the parabola are summarized in Tab. 2.

2.3 Shower lateral dispersion

Photons and electrons can be distinguished from hadrons by the difference in the shape of the showers which develop in the calorimeter. In addition, high-p_T π^0 which are detected through their two decay-photons merging into a single electromagnetic cluster in the calorimeter can furthermore be distinguished from photons up to a limiting p_T value of about 100 GeV/c. We characterize the shower by its lateral dispersion[7] and we calculated the probability density distribution, $P(dis\,|\,i)$, for photons, hadrons and high-p_T π^0 shown

[7]Different shower parameters can be used [4, 7]. The most significant ones are the main axis of the shower ellipse and the lateral dispersion. Both parameters provide similar results.

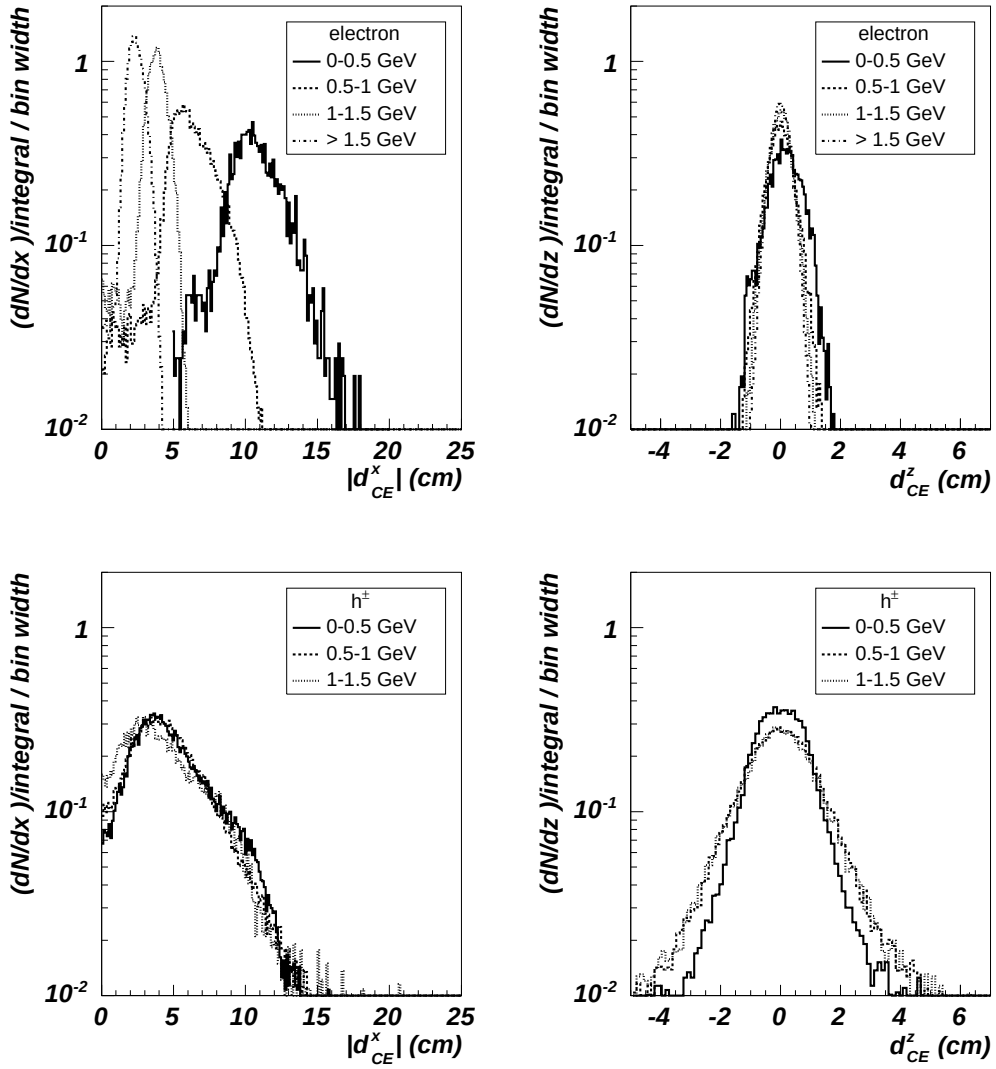

Figure 3: Probability density distributions of the distance between the impact on CPV and on EMC projected on the surface on PHOS along the x-axis (left) and z-axis (right) measured for electrons (upper), and charged hadrons (p, $\bar{p}$, $\pi^{\pm}$ and $k^{\pm}$, lower) and for different reconstructed energies.

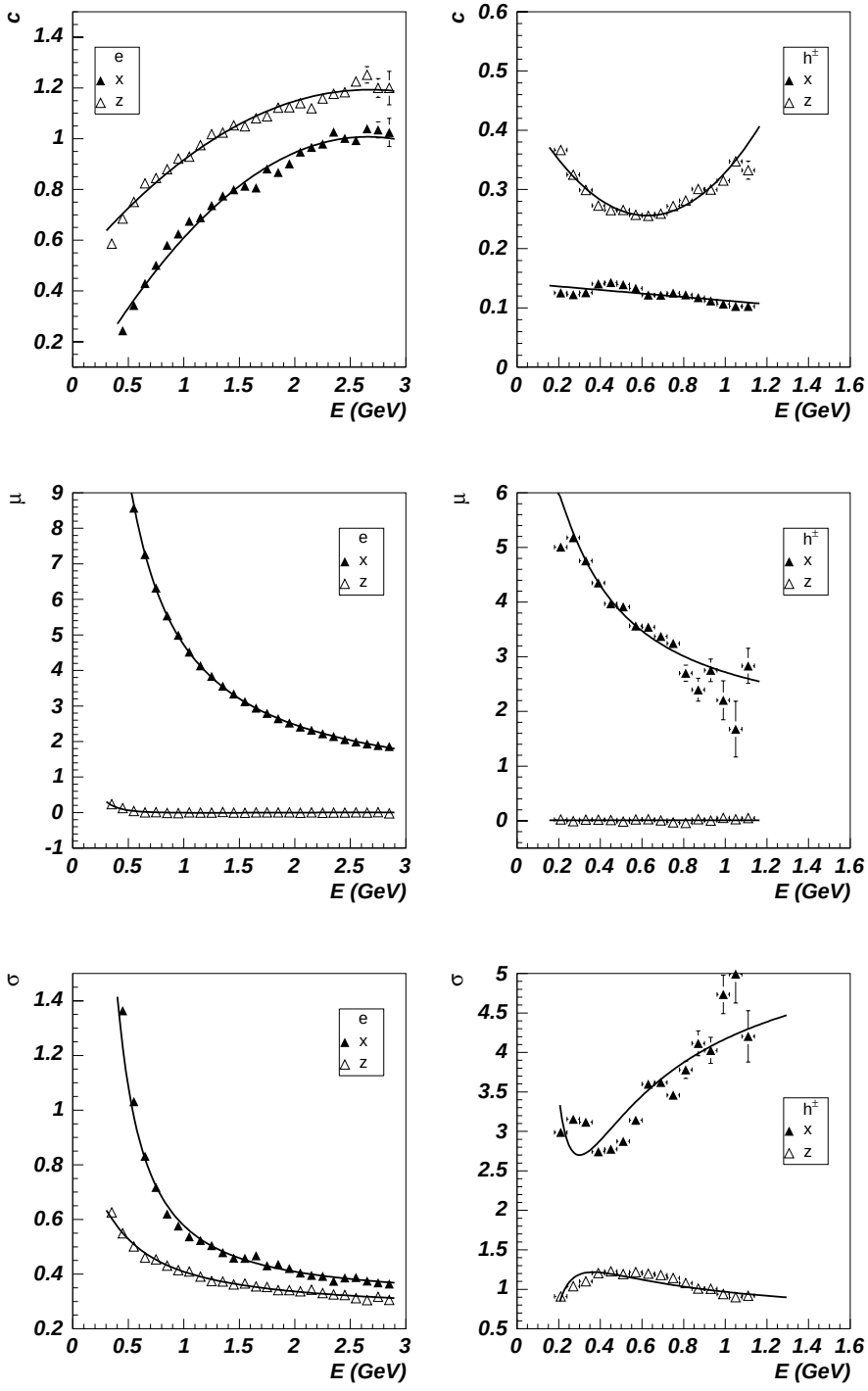

Figure 4: Parameterization of the reconstructed energy dependence of the probability density distributions calculated for charged hadrons and electrons and for the x- and z-component of the distance between the impact on CPV and on EMC. Left figures are for electrons and the right ones for charged hadrons (p, $\bar{p}$, $\pi^{\pm}$ and $k^{\pm}$).

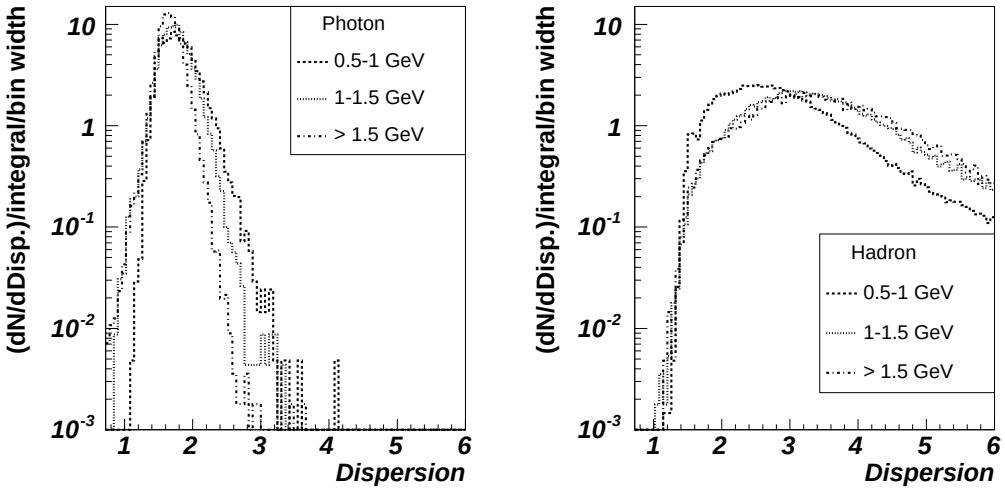

Figure 5: Probability density distributions of the shower lateral-dispersion measured for photons (left) and hadrons (right) and for different reconstructed energies.

in Fig. 5.

The lateral dispersion is not significant when the cluster multiplicity (number of hit calorimeter cells which contribute to the cluster) is below four. For photons with reconstructed energies below 0.5 GeV, the average number of clusters is three (Fig. 6), setting the limit of applicability of this selection criterion.

The probability density distribution is parameterized by Gaussian distributions for photons and high-p_T π^0 and by Landau distributions for hadrons. The energy dependence of the Gaussian or Landau parameters (Fig. 7) is described by a polynomial function of $1/E$, $p_0 + p_1/E^2 + p_2/E$, for the μ and σ parameters and the constant parameter by a parabola. The parameters of the polynomial and the parabola are summarized in Table 3.

3 PID weight

From the probability density distributions calculated for particles of type γ, $e^{\pm}$, h^0, $h^{\pm}$ and high-p_T π^0 and parameterized as described in the previous section, and for each measured reconstructed particle characterized by a *tof* value, a d_{CE} value and a *dis* value, a PID weight, ranging from 0 to 1, is calculated as follows:

- Given the *tof* value of the reconstructed particle, the probabilities $P(tof \mid i)$ are derived from the pre-established distributions (Sec. 2.1). For reconstructed energies larger than 2 GeV $P(tof \mid i)$ are set to 1.

- Given the d_{CE} value measured along the x and z-axis, the probabilities density, $P(d_{CE}^{xz} \mid i)$ are calculated as the product $P(d_{CE}^{x} \mid i) \cdot P(d_{CE}^{z} \mid i)$, of the pre-established

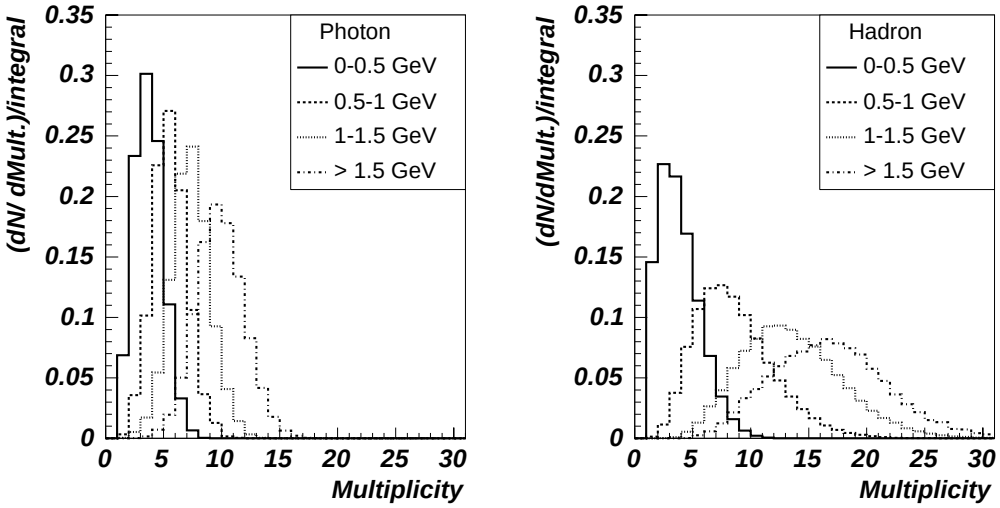

Figure 6: Cluster multiplicity measured with PHOS for photons (left) and hadrons (right) with different reconstructed energies.

	p_0	p_1	p_2
		photon	
c	1.5	0.49	$-1.7 \cdot 10^{-2}$
μ	1.5	$4.0 \cdot 10^{-2}$	0.21
σ	$4.8 \cdot 10^{-2}$	-0.12	0.27
	high-p_T	π^0	
c	0.25	$3.3 \cdot 10^{-2}$	$-1.0 \cdot 10^{-5}$
μ	1.50	398	12
σ	$-7.0 \cdot 10^{-2}$	-524	22
		hadron	
c	6.5	-5.3	1.5
μ	3.8	0.23	-1.2
σ	0.88	$9.3 \cdot 10^{-2}$	-0.51

Table 3: Parameters of the energy dependence of the probability density distributions calculated for charged hadrons and electrons and for the shower lateral dispersion.

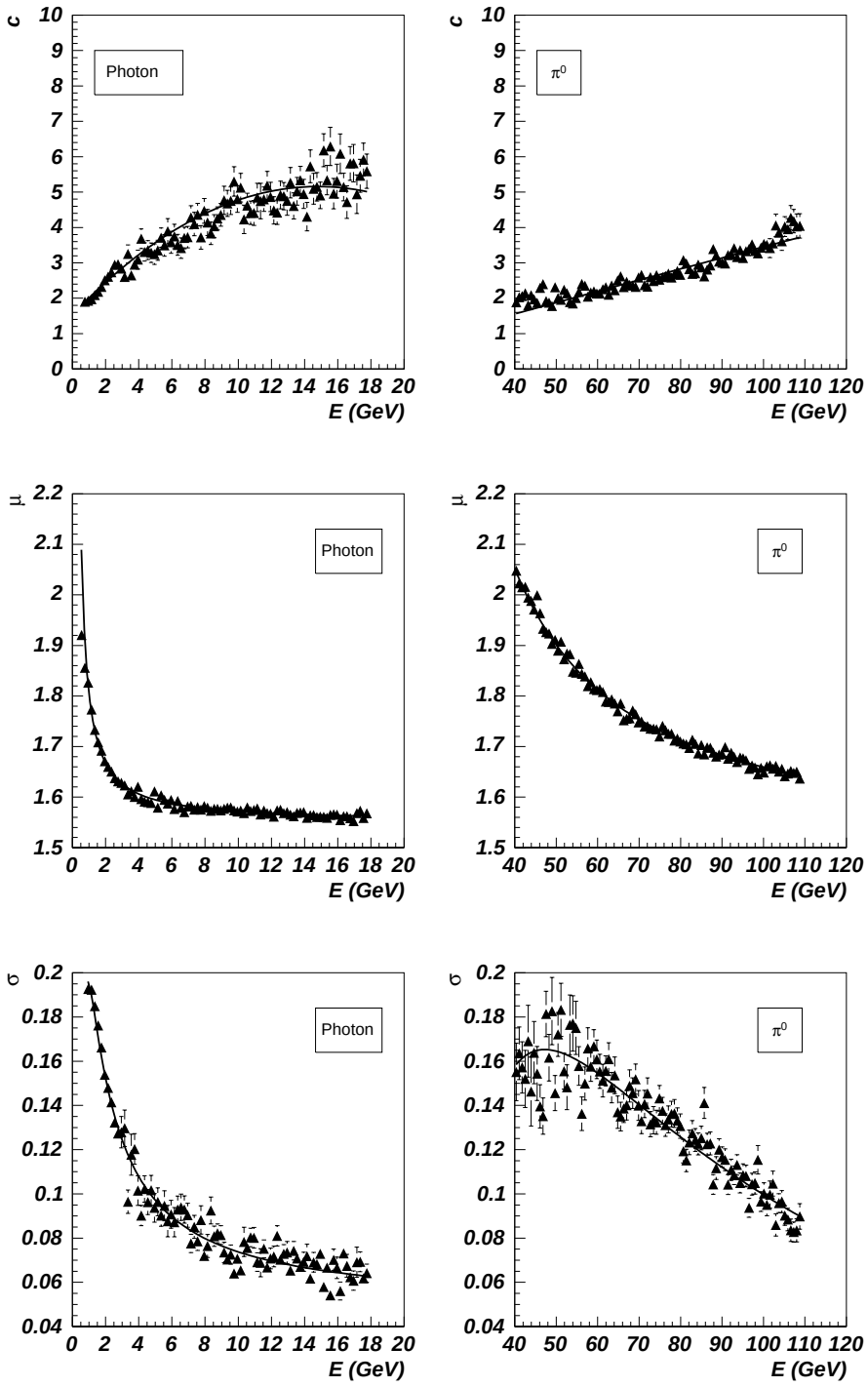

Figure 7: Parameterization of the reconstructed energy dependence of the probability density distributions calculated for the shower lateral-dispersion and for photons (left) and high-p_T π^0(right).

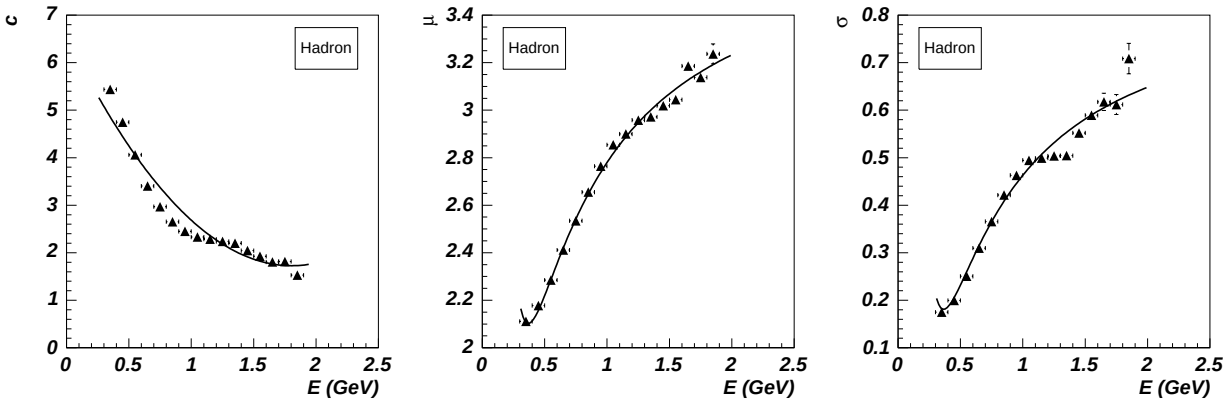

Figure 8: Parameterization of the reconstructed energy dependence of the probability density distributions calculated for the shower lateral dispersion and for hadrons.

distributions (Sec. 2.2). A particle is identified as a neutral particle if

$$\max\left[P(d_{CE}^{xz} \mid e^{\pm}),\, P(d_{CE}^{xz} \mid h^{\pm})\right] < 10^{-5},$$

and $P(d_{CE}^{xz}|\gamma), P(d_{CE}^{xz}|h^0)$, and$P(d_{CE}^{xz}|\pi^0)$ are set to 1 and $P(d_{CE}^{xz}|e^{\pm})$ and $P(d_{CE}^{xz}|h^{\pm})$ to 0. If the particle is not found to be a neutral particle $P(d_{CE}^{xz} \mid \gamma)$, $P(d_{CE}^{xz} \mid h^0)$ and $P(d_{CE}^{xz} \mid \pi^0)$ are set to 0.

- Given the *dis* value of the reconstructed particle, the probabilities $P(dis \mid i)$ are derived from the pre-established distributions (Sec. 2.3). If the cluster multiplicity is smaller than four and the reconstructed energy is smaller than 0.5 GeV, then $P(dis \mid i)$ is set to 1. The high-p_T π^0 identification is only possible for $E_{rec} > 30$ GeV (energy for which the two decay photons merge into a single cluster in PHOS), for reconstructed energies below this value, $P(dis \mid \pi^0)$ is set to 0.

- The probability that a hadron develops a shower in PHOS is also taken into account. This probability depends on the initial hadron energy and a hadron type, and as an upper limit it was calculated from the response function of PHOS to mono-energetic charged pions of 100 GeV (Fig. 9). The response, normalized to one, gives the probability density distributions $P(\mathrm{rec} \mid i)$ which are tentatively parameterized by $0.32 \cdot e^{-3.8E} + 0.0054 \cdot e^{-0.056E}$ for $h^{0,\pm}$ and set to 1 for γ, $e^{\pm}$ and high-p_T π^0.

- Finally, the PID weight, $W(i)$, for particle species i is calculated as the product of the four probability density distributions for the particle i normalized to the sum of these products for all the particle species, being $s = \gamma$, $e^{\pm}$, h^0, $h^{\pm}$ and high-p_T π^0,

$$W(i) = \frac{P(tof \mid i) \cdot P(d_{CE}^{xz} \mid i) \cdot P(dis \mid i) \cdot P(\mathrm{rec} \mid i)}{\sum_s \left[P(tof \mid s) \cdot P(d_{CE}^{xz} \mid s) \cdot P(dis \mid s) \cdot P(\mathrm{rec} \mid s)\right]}. \qquad (2)$$

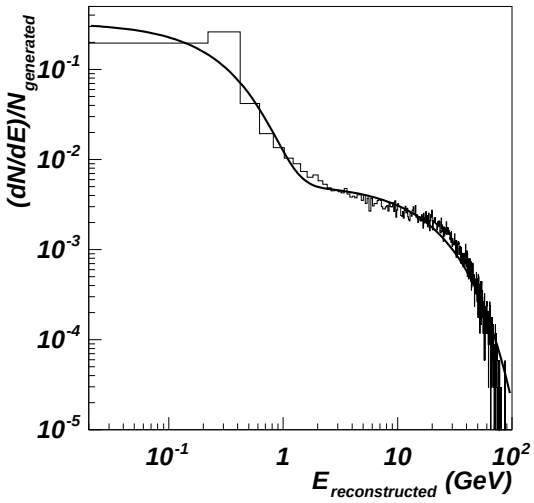

Figure 9: Simulated PHOS response function to 100 GeV/c $\pi^{\pm}$.

4 PID efficiency and contamination

We have applied this PID procedure to single photons, electrons and π^0, generated with an uniform energy distribution, merged or not into HIJING events (Pb-Pb collisions at 5.5A TeV, $b < 2$ fm) mimicking the heavy-ion collision (HIC) environment. Without the HIJING event, photons reconstructed with energies below 30 GeV are well identified with a PID weight equal to 1 (Fig. 10). For energies below 0.5 GeV, where the shower shape criterion is not effective, the neutral hadron weight becomes large, i.e., photons can be misidentified as neutral hadrons. For energies larger than 30 GeV, photons can be misidentified as high-p_T π^0. This misidentification probability increases with increasing reconstructed energy. Electrons are usually well identified with a weight equal to one for reconstructed energies larger than 0.5 GeV. These results are slightly changed when a single particle is merged into a HIJING event (Fig. 11) with the weight distributions becoming wider at low energies and the peak at a weight equal to 0 is shifted to higher energies. For single and merged high-p_T π^0, with reconstructed energies in the range $30 < E_{rec} < 120$ GeV (Fig. 12), the PID photon weight is significant and increases with the reconstructed energy.

Applying the procedure to all detected particles in HIJING events (Fig. 13), photons, neutral hadrons and charged hadrons are well identified.

We define the PID efficiency as the probability to correctly identify particles of type i, i.e., the ratio of the spectrum of reconstructed clusters generated by the particles of type i, and identified with a PID weight, $W(i)$, larger than a given threshold value, $W^{th}(i)$, and of the spectrum of all reconstructed clusters generated by the same type of particles, without condition on $W(i)$. Two energy bins have been considered: particles with energy ranging from 0 to 5 GeV and particles with energy ranging from 5 to 120 GeV (from 30

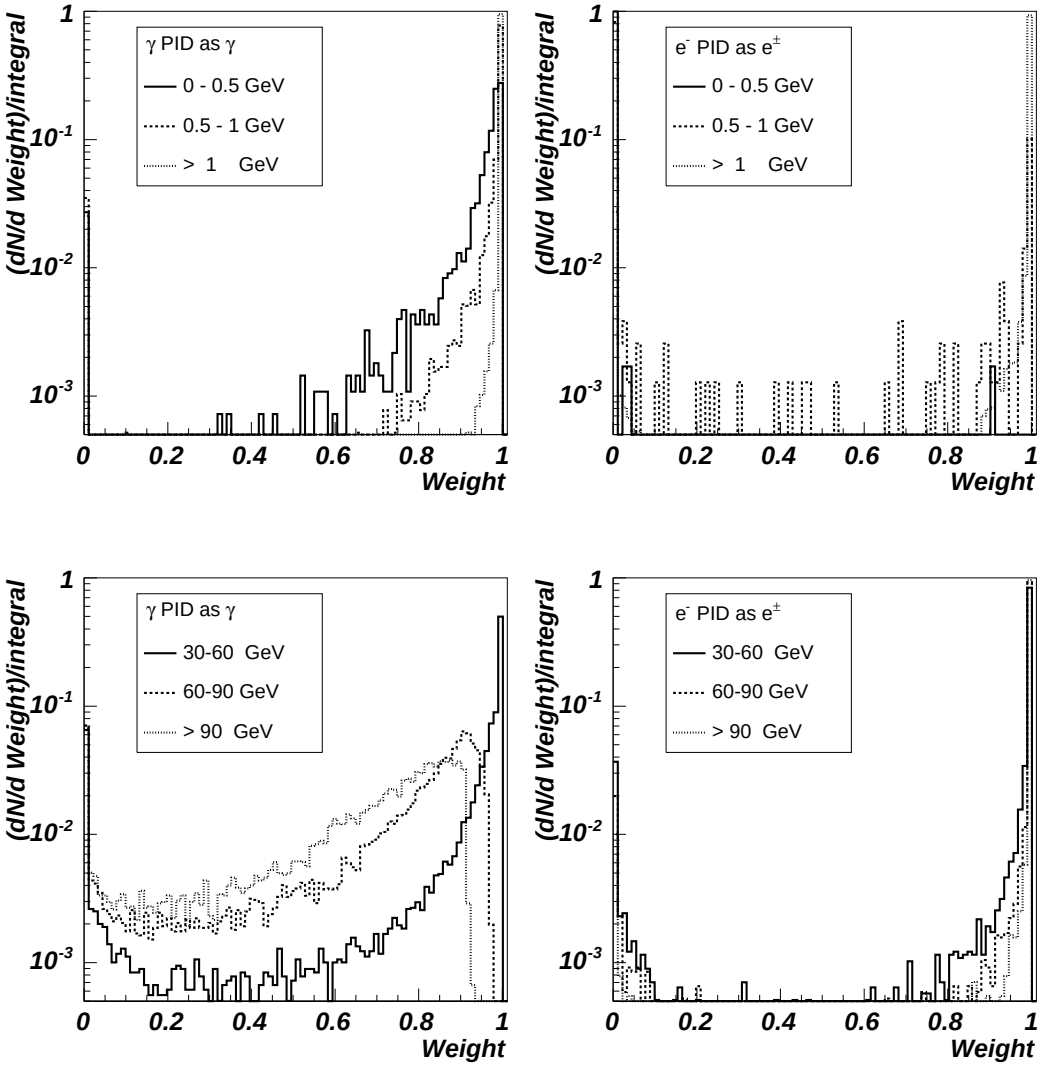

Figure 10: Distributions of PID weights calculated for single photons (left) and electrons (right) and for different reconstructed energy bins. Upper (lower) frames: photons and electrons were generated with an uniform energy distribution between 0 (5) and 5 (120) GeV.

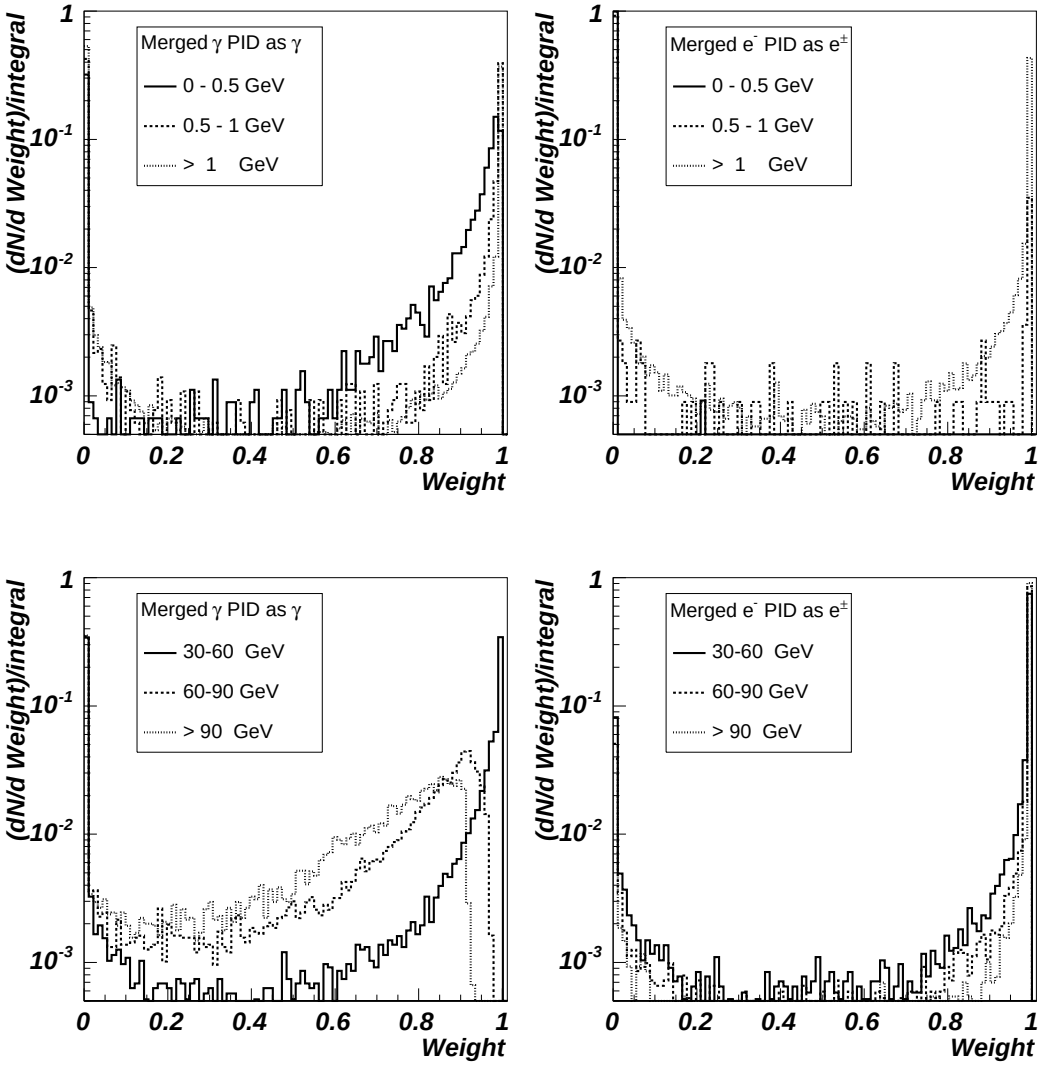

Figure 11: Distributions of PID weights calculated for single photons (left) and electrons (right) merged into HIJING events (Pb-Pb collisions at $5.5A$ TeV, $b < 2$ fm) and for different reconstructed energy bins. Upper (lower) frames: photons and electrons were generated with an uniform energy distribution between 0 (5) and 5 (120) GeV.

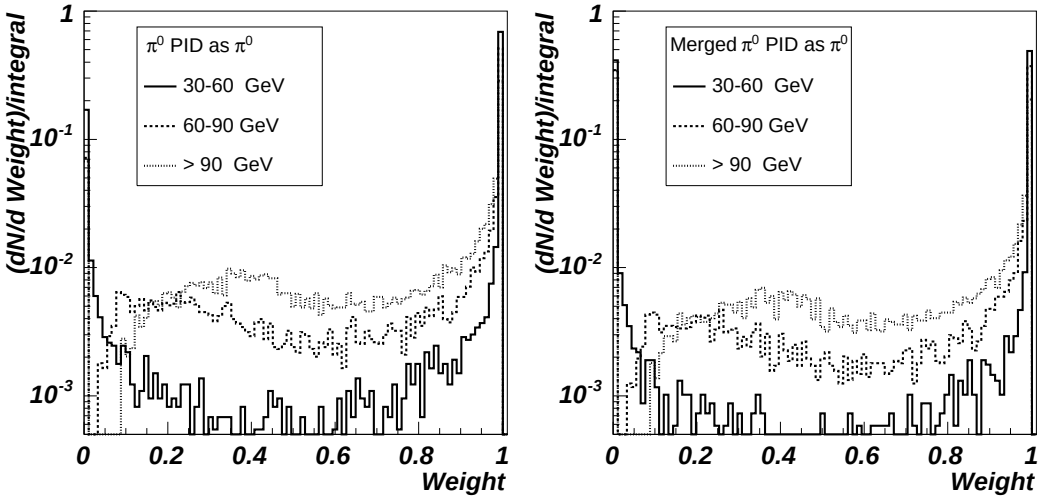

Figure 12: Distributions of PID weights calculated for high-p_T π^0 and for different reconstructed energy bins. Neutral pions were generated with an uniform energy distribution between 30 and 120 GeV. Left frame: single π^0 case. Right frame: case of a π^0 merged into HIJING events (Pb-Pb collisions at 5.5A TeV, $b < 2$ fm).

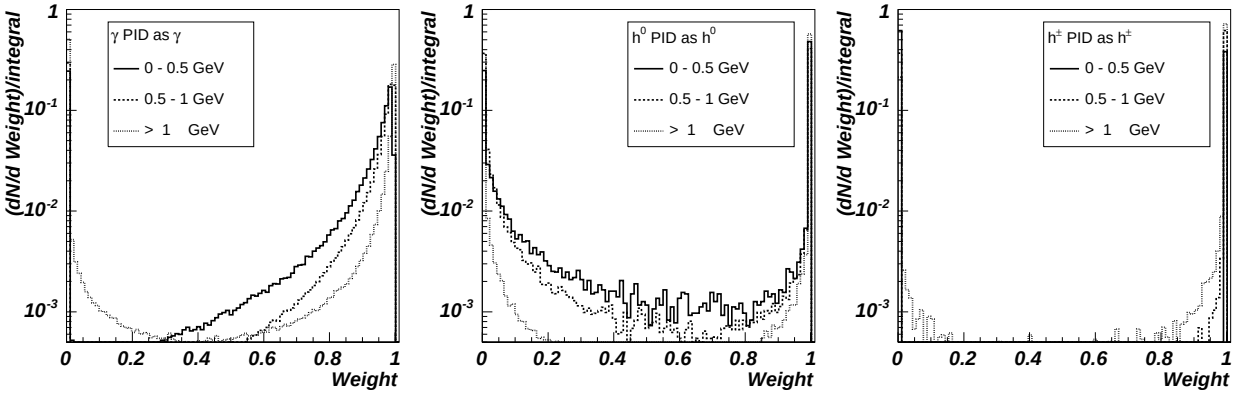

Figure 13: Distributions of PID weights calculated for photons (left), neutral hadrons (middle) and charged hadrons (right) and for different reconstructed energy bins. These particles were taken from HIJING events (Pb-Pb collisions at 5.5A TeV, $b < 2$ fm).

to 120 GeV for π^0).

The contamination is defined as the ratio of the spectrum of reconstructed clusters not generated by particles of type i, but identified as particle of type i, and of the spectrum of all reconstructed clusters identified as particles of type i.

4.1 Low-energy particles

Single electrons and photons are identified with an almost 100 % efficiency (Fig. 14) for particles reconstructed with energies larger than 1 GeV. This efficiency decreases to about 40-50 % when photons and electrons are merged into central HIJING events ($b < 2$ fm). A small dependence with $W^{th}(i)$ is observed.

Comparing the efficiencies obtained for single particles with uniform energy distribution merged into HIJING events (Fig. 14) with the efficiency obtained for the particles in the HIJING events with a realistic energy distribution (Fig. 15), we observe an important difference, attributed to the difference in shape (uniform versus exponential) of the energy spectrum and to overlapping clusters. Indeed, the decrease of the efficiency from about 70 % $\left[W^{th}\left(i\right) = 0.05\right]$ down to about 50 % with increasing reconstructed energy (Fig. 14) is explained by the fact that the overlapping clusters give a too high reconstructed energy, distorting the reconstructed spectrum, and the shower shape gives a wrong information on the particle type. When realistic spectral shapes are considered (Fig. 15), the efficiency drops even faster down to a minimum value of about 20 %, due to the exponential shape of the generated particle spectrum. These efficiency variations are attenuated when considering events with lower particle multiplicities as can be seen for less central HIJING events, $b < 5$ fm, (Fig. 16).

The contamination of wrongly identified particles in HIJING events (Figs. 15 and 16) does not show a strong variation nor with reconstructed energy nor with the event particle-multiplicity and is small, ranging from 3.5 to 1.5 % in the $b < 2$ fm case and from 2.5 to 1 % in the $b < 5$ fm case.

4.1.1 Comparison with PCA method

An alternative PID method, based on the Principal Component Analysis (PCA), has been developed earlier [4,7]. Within this approach, three classes of PID are defined according to the purity level: low, medium and high purity. We obtained single photon PID efficiencies of 90 %, 80 % and 40-50 %, for the three purity classes. These values are to be compared to the almost 100 % efficiency obtained with the Bayesian method independent of the value of $W^{th}(i)$, used to select photons. In the HIC environment, the efficiencies obtained for both methods are reduced to less than 50 % while the contamination of wrongly identified hadrons is of the order of a few % depending on the purity class in the PCA method and on the $W^{th}(i)$ value in the Bayesian method.

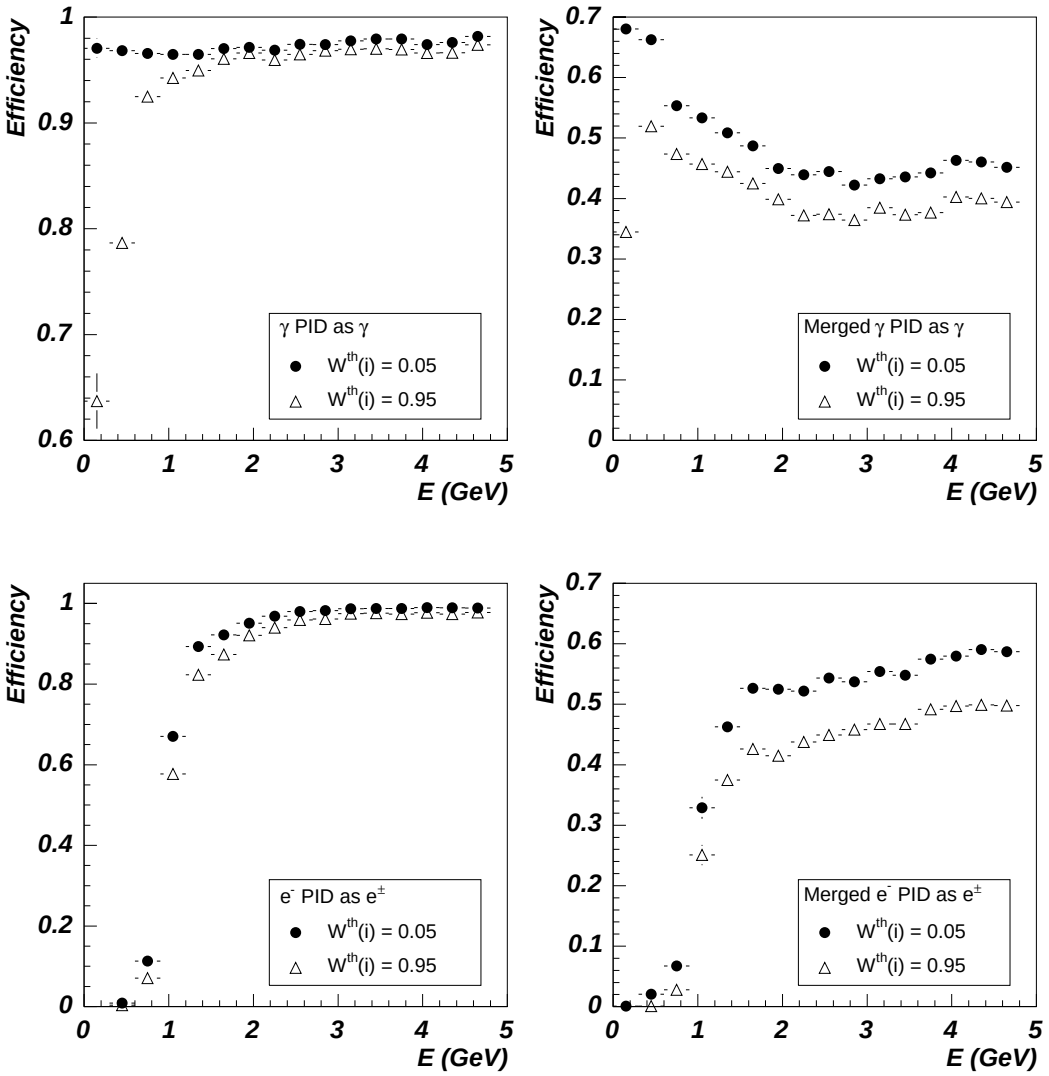

Figure 14: PID efficiency for photons (upper) and electrons (lower) as a function of the reconstructed energy. Right frames: efficiency for single particles, left frames: particles merged into HIJING events (Pb-Pb collisions at $5.5A$ TeV, $b < 2$ fm). Particles were generated with an uniform energy distribution between 0 and 5 GeV.

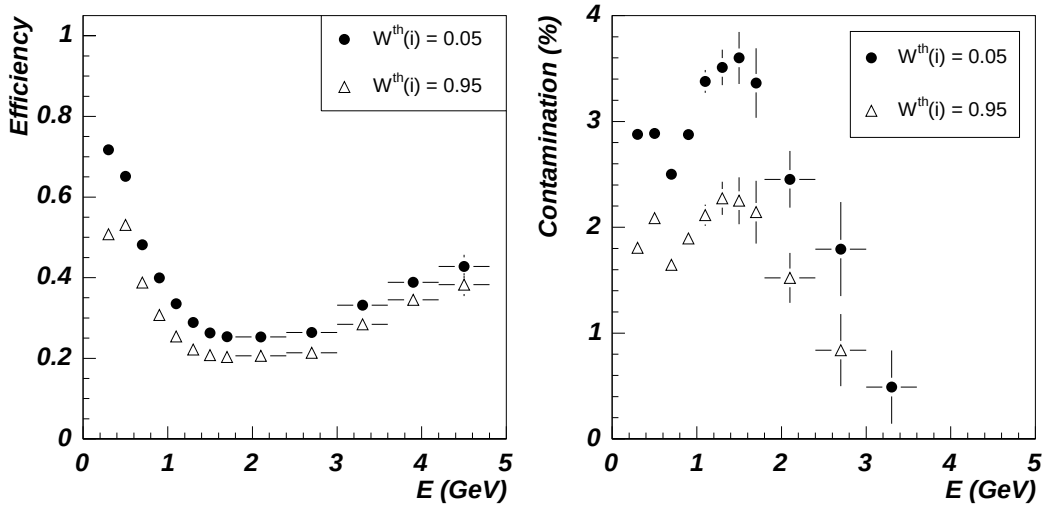

Figure 15: PID efficiency for photons with an exponential energy spectrum in HIJING events (Pb-Pb collision at 5.5A TeV, $b < 2$ fm). Left frame: photon PID efficiency as a function of the photon reconstructed energy. Right frame: Contamination of wrongly identified photons as a function of the particle reconstructed energy.

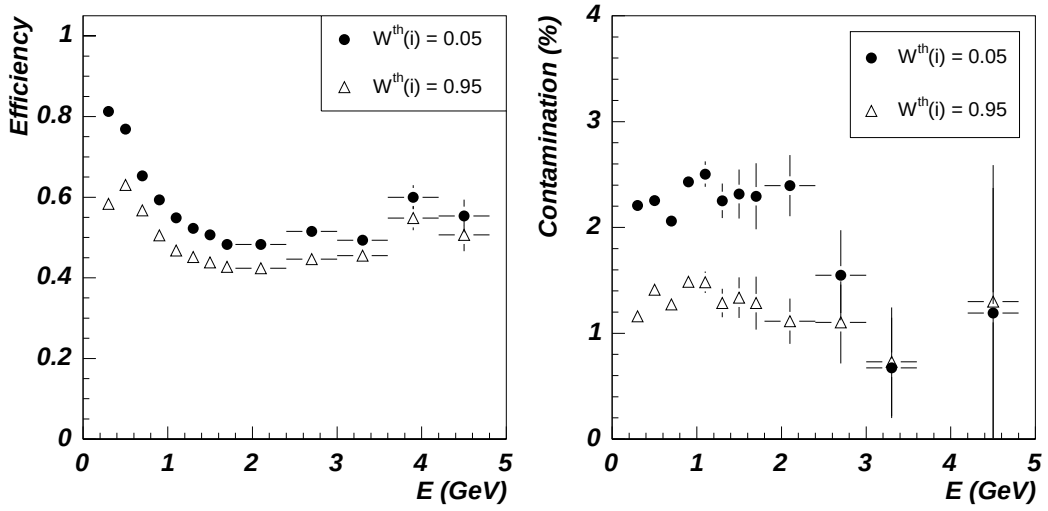

Figure 16: PID efficiency for photons with an exponential energy spectrum in HIJING events (Pb-Pb collision at 5.5A TeV, $b < 5$ fm). Left frame: photon PID efficiency as a function of the photon reconstructed energy. Right frame: Contamination of wrongly identified photons as a function of the particle reconstructed energy.

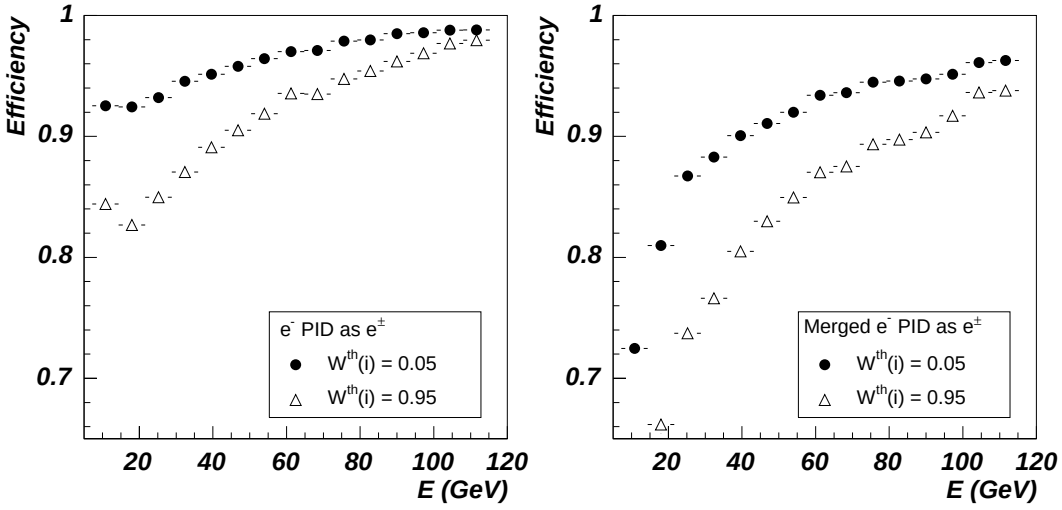

Figure 17: PID efficiency for high-energy electrons as a function of the reconstructed energy. Left: single electrons, right: electrons merged in HIJING events (Pb-Pb collisions at 5.5A TeV, $b < 2$ fm).

4.2 High-energy particles

The PID efficiency obtained for high energy particles from 0 to 120 GeV (neutral pions from 30 to 100 GeV) show only a small dependence with the value of $W^{th}(i)$ for single electrons (Fig. 17). The PID efficiency for single electrons is larger than 85 % and is reduced by 5-10 % when electrons are merged in a HIC environment.

The PID efficiency for high-energy photons (Fig. 18) is the same as the one obtained for low-energy photons ($2 < E_{rec} < 5$ GeV) up to reconstructed energies of 30 GeV. Beyond 30 GeV, the contribution of photons wrongly identified as π^0 becomes important showing a strong dependence with the $W^{th}(i)$ value.

In order to find the optimum value of $W^{th}(i)$, the following PID efficiency ratios have been minimized, the probability of the photon misidentification as a π^0

$$\frac{\epsilon(\gamma \,\mathrm{as}\, \pi^0)}{\epsilon(\gamma \,\mathrm{as}\, \pi^0) + \epsilon(\gamma \,\mathrm{as}\, \gamma)} \tag{3}$$

and the probability of the π^0 misidentification as a photon

$$\frac{\epsilon(\pi^0 \,\mathrm{as}\, \gamma)}{\epsilon(\pi^0 \,\mathrm{as}\, \gamma) + \epsilon(\pi^0 \,\mathrm{as}\, \pi^0)}, \tag{4}$$

and the minimization were taken against the values of $W^{th}(i)$ (Fig. 19).

The optimum value of $W^{th}(i)$ is calculated (Fig. 20) for photons with the following parameterization

$$f(E) = 0.98 + 6.0 \cdot 10^{-3} \cdot E - 2.0 \cdot 10^{-4} \cdot E^2 + 1.1 \cdot 10^{-6} \cdot E^3, \tag{5}$$

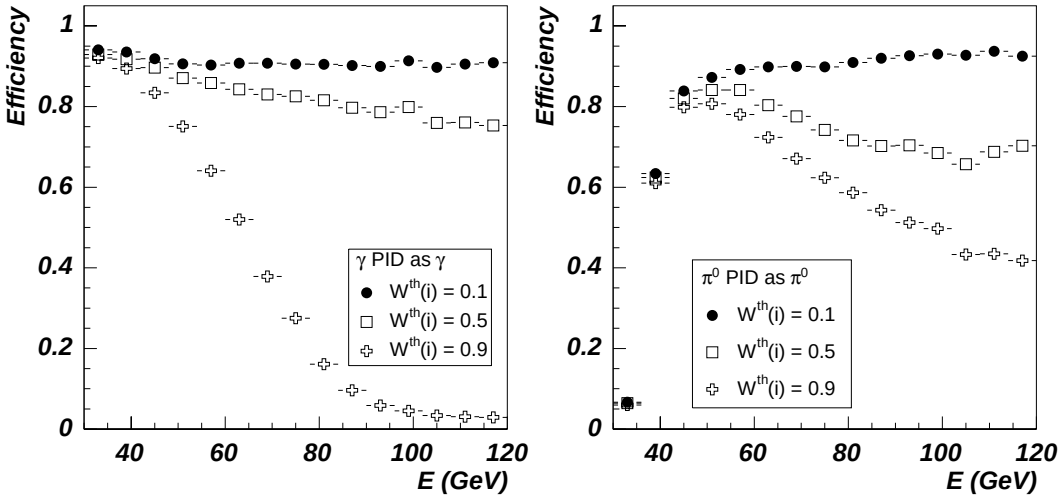

Figure 18: PID efficiency as a function of the reconstructed energy for single high-energy photons (left) and π^0 (right).

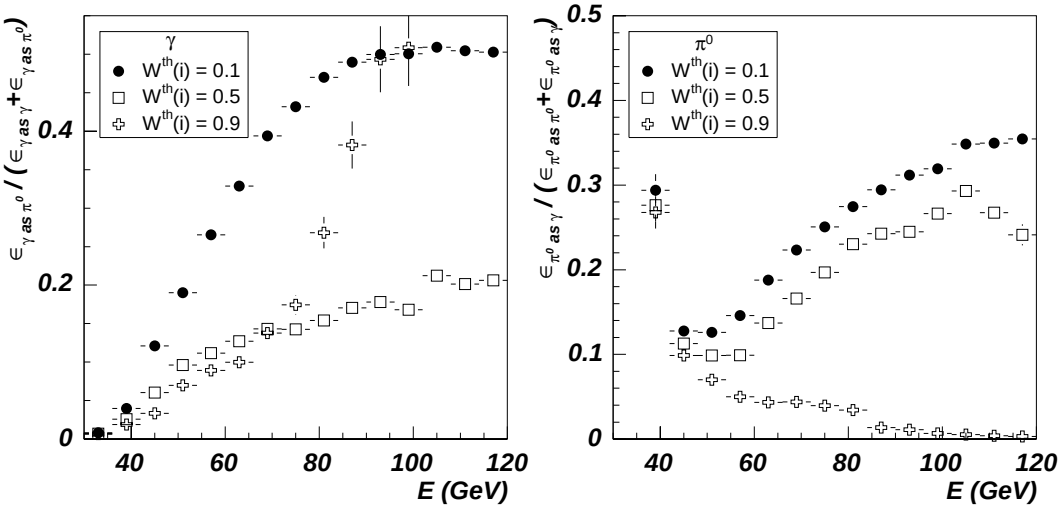

Figure 19: PID efficiency ratios defined in Eq. (3) (left) and Eq. (4) (right) as a function of the reconstructed energy for three different values of $W^{th}(i)$. Photons are generated with an uniform energy distribution between 5 and 120 GeV (left) and π^0 between 30 and 120 GeV (right).

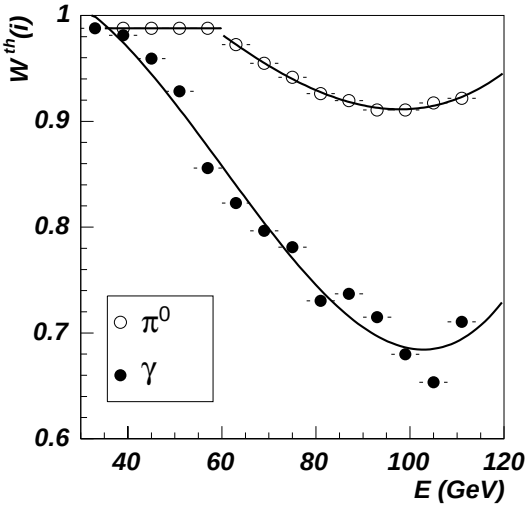

Figure 20: Values of $W^{th}(i)$ for which the ratios of Eq. (3) (•) and Eq. (4) (∘) are minimum. Points were fitted by a third order polynomial for photons [Eq. (5)] and for π^0 [Eq. (6)] .

and for π^0, from:

$$f(E) = 1.18 - 1.95 \cdot 10^{-3} \cdot E - 4.31 \cdot 10^{-5} \cdot E^2 + 3.61 \cdot 10^{-7} \cdot E^3, \tag{6}$$

and for the energy range between 60 and 120 GeV. For smaller energies, the optimum value is $W^{th}(i) = 0.98$.

Using the values of $W^{th}(i)$ deduced in this way, the final PID efficiency and contamination of wrongly identified particles are calculated (Fig. 21). Assuming that photons and π^0 are produced in the HIC in the same amount, background-to-signal ratios have been constructed (Fig. 22). For photons, the background (π^0 identified as photon) to signal (photons identified as photons) is smaller than 0.2 independent of the fact that photons are within a HIC environment or not. The ratio however changes strongly with the photon reconstructed energy.

In Refs. [4, 7], alternative identification methods to distinguish high energy photons from neutral pions were developed. They are based on an one-dimensional shower shape analysis and they give similar results than the present method.

Conclusion

We have developed an algorithm to identify on an event-by-event basis photons, electrons and high-energy neutral pions detected with the photon spectrometer PHOS of the ALICE experiment. The method is based on the Bayes theory of probabilities, and is compatible with the global PID involving the central tracking detectors of ALICE. We obtain excellent PID efficiencies, close to 100 %, for photons and electrons in the energy range from 0.5 GeV

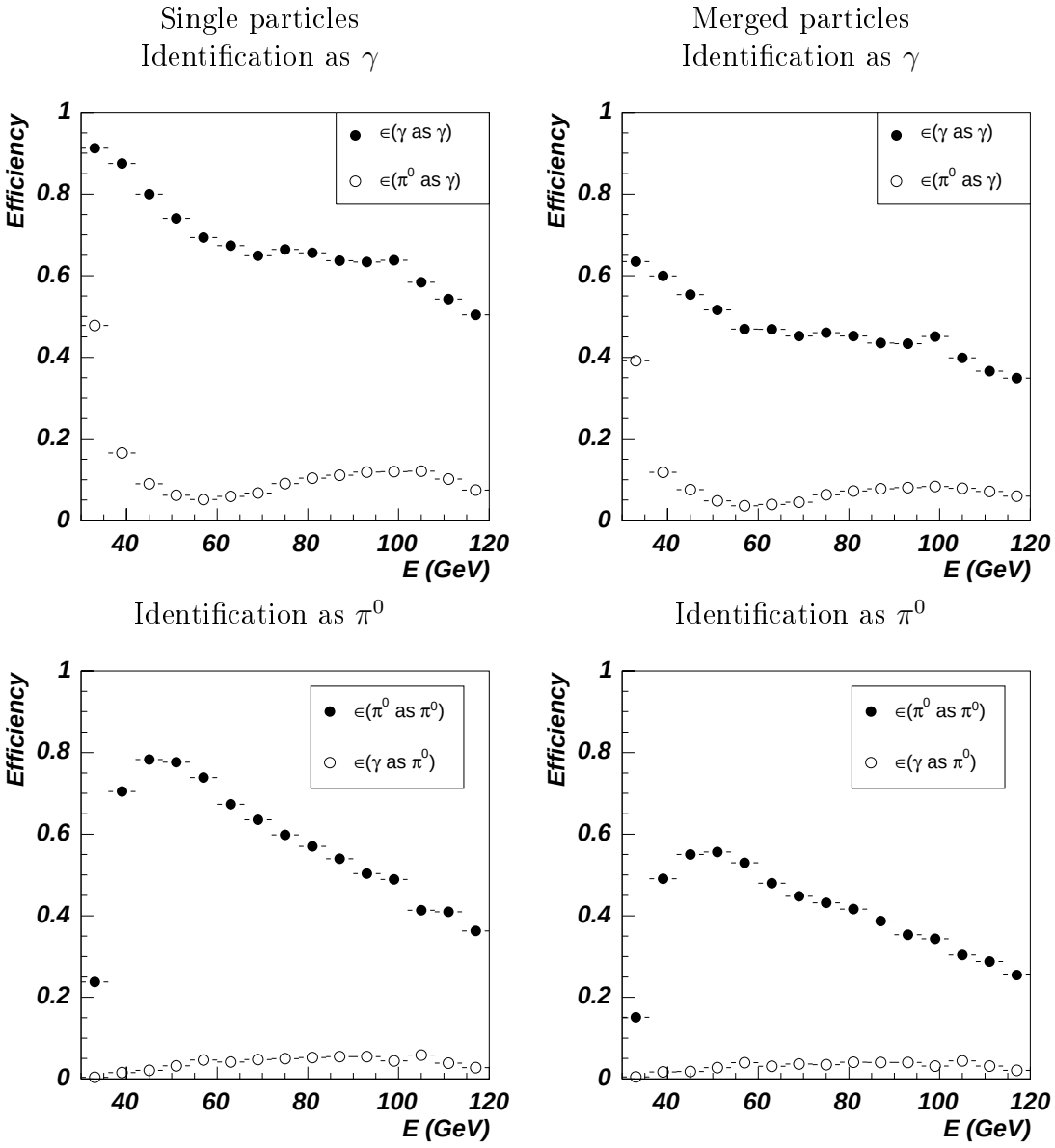

Figure 21: PID efficiency for a single high-energy photon or π^0 to be identified as a hard photon [$W^{th}(i)$ given by Eq. (5) (upper)] or as a hard π^0 [$W^{th}(i) = 0.98$ for $E < 60$ GeV , and $W^{th}(i)$ given by Eq. (6) for $E > 60$ GeV (lower)] as a function of the particle reconstructed energy. Right: for single particles, left: for particles merged into HIJING events (Pb-Pb collisions at $5.5A$ TeV, $b < 2$ fm). Photons are generated with an uniform energy distribution between 5 and 120 GeV for photons, and between 30 and 120 GeV for π^0.

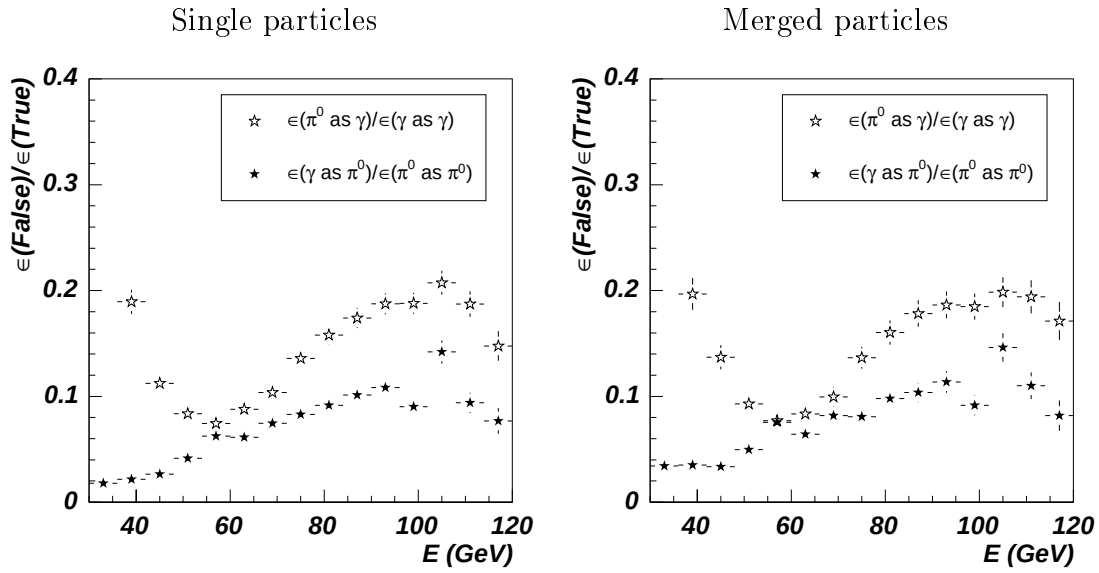

Figure 22: Ratios of the PID contamination of wrongly identified hard $\pi^0(\gamma)$ to the PID efficiency of γ (π^0) as a function of the reconstructed energy. $W^{th}(i)$ given by Eq. (5) for photon PID. For π^0 PID, $W^{th}(i)$ given by Eq. (6) for $E > 60$ GeV, and $W^{th}(i) = 0.98$ for $E < 60$ GeV. Right: for single particles. Left: for particles merged with a HIJING event (Pb-Pb collisions at $5.5A$ TeV, $b < 2$ fm). Photons are generated with an uniform energy distribution between 5 and 120 GeV for photons, and between 30 and 120 GeV for π^0.

(1 GeV for electrons) to 120 GeV in a particle free environment. In HIC environment (HIJING simulations with $b < 2$ fm), the PID efficiencies are reduced only by 10-20% except for low energy particles (0.5 - 5 GeV) for which the efficiency is reduced by 50 %, due mainly to the imperfect matching for between the CPV and EMC reconstructed points. It is worthwhile noticing the achieved low level of contamination from wrongly identified hadrons, as low as a few %. Neutral pions with energy larger than 30 GeV, when the two decay photons merge into a single cluster in PHOS, can be identified as well. In a particle-free environment, the photon PID efficiency varies from 90 to 50 % and the π^0 PID efficiency from 80 to 40 % when the reconstructed energy increases. The contamination of wrongly identified particles, π^0 identified as photons, stays low varying from 5 % to 10 % and photons identified as π^0 stays below 5 %. The HIC environment reduces the PID efficiencies by only 10 %. These results confirm the ability of PHOS to identify direct photons and reduce the contamination due to wrongly identified π^0 to a sufficiently low level to obtain a large direct photon signal over the decay photon background. This work was supported by the FPI grant FP2000-5452 from the Spanish Ministry of Education and Science, the INTAS grant 03-52-5747 and the EU program HPMT-CT-2001-00346.

References

[1] ALICE-PHOS Collaboration, ALICE TDR **2** (1999), *PHOS Technical Design Report.*

[2] A. Blick *et al.*, ALICE Note **ALICE-INT-2000-021** (2000).

[3] G. Conesa *et al.*, Nuc. Ins. Met. **A 537** (2005).

[4] ALICE-PHOS Collaboration, Chap. 5 of ALICE Physics Performance Report http://alice.web.cern.ch/Alice/ppr/chap5dir/neutral/alice_chap5_neutral.ps.

[5] ALICE Collaboration, J. Phys. G: Nucl. Part. Phys. **30**, 1517 (2004).

[6] M. Bogolyubsky *et al.*, Tech. Exp. Tech. **45**, 327 (2002).

[7] G. Conesa Balbastre, Ph.D. Thesis: *Identification of particles and hard processes with the spectrometer PHOS of the ALICE experiment*, 2005.

[8] M. Bogolyubsky, Y. Kharlov, and S. Sadovsky, ALICE Note **ALICE-INT-2003-037** (2004).

[9] AliRoot: ALICE offline project, http://aliceinfo.cern.ch/Offline.

[10] ROOT, http://root.cern.ch/.

[11] M. Gyulassy and X.-N. Wang, Comput. Phys. Commun. **83**, 307 (1994).